ChemElectroChem

Research Article
doi.org/10.1002/celc.202300383

Chemistry Europe
European Chemical Societies Publishing

www.chemelectrochem.org

Performance of Transition Metals in Imidazolium-Assisted CO_2 Reduction in Acetonitrile

Sobhan Neyrizi,[a, b] Mark A. Hempenius,[b] and Guido Mul*[a]

This study explores the electrochemical reduction of CO_2 in dry acetonitrile containing 1,3-dimethyl imidazolium cations, utilizing late-transition metals (Au, Ag, Zn, Cu, and Ni). All metals exhibit remarkable selectivity, nearing 100%, for CO formation. Particularly noteworthy is Au, which manifests the lowest (−2.37 V vs. Ag/Ag^+) overpotential in chronopotentiometry experiments. We propose that, for metals with lower CO binding energies compared to Au (Ag and Zn electrodes) – calculated by DFT, the rate-determining step is the adsorption of CO_2. This distinction in CO_2 adsorption is reinforced by the examination of partial charge transfer from negatively charged slabs to CO_2 (−0.241 a.u with the Au electrode and +0.002 a.u with the Zn electrode). Conversely, the greater CO binding energy calculated for Cu and Ni likely diminishes electrocatalytic activity relative to the Au electrode. Our results unveil a volcano trend in catalyst activity, albeit with smaller performance disparities between the late-transition metals and Au than previously observed in aqueous conditions, possibly due to the co-catalytic influence of imidazolium cations. This study suggests that metals unsuitable for aqueous environments hold promise for cost-effective and viable electrochemical conversion of CO_2 to CO in non-aqueous media containing imidazolium compounds.

Introduction

Over the years, substantial progress has been made in optimizing electrode properties for electrochemical reduction of CO_2, as well as electrode design, and electrolyte composition.[2] However, despite these advancements, several challenges still limit the commercial viability of this technology, particularly when employing aqueous electrolytes.[3] Despite the apparent advantages of aqueous electrolytes (sustainability, low resistivity at high salt concentrations), one of the key challenges associated with aqueous electrolytes is the low solubility of CO_2.[4] Additionally, the dissolution of CO_2 in water leads to acidification of the electrolyte, accompanied by the formation of bicarbonate/carbonate species and the potential precipitation of associated salts.[5] These factors, combined with the competing hydrogen evolution reaction and the instability of metal and metal oxide catalysts in aqueous electrolytes, pose significant challenges.[6] To address these challenges, the use of non-aqueous solvents, notably acetonitrile, has emerged as a promising alternative.[4a,c, 7] Acetonitrile exhibits up to 8 times higher CO_2 solubility compared to water, making it an attractive choice for CO_2 electrochemical reduction.[8] Moreover, acetonitrile provides enhanced electrode stability against dissolution.

However, solvent oxidation at the anode should be prevented, and to enhance electrochemical performance in non-aqueous media, the addition of cations becomes necessary. These cations serve the dual purpose of reducing resistance of acetonitrile solutions and promoting CO_2 conversion. Particularly, imidazolium cations have been shown to enhance the performance of electrodes for CO_2 reduction in non-aqueous media.[9] In our recent study, we investigated the effect of the molecular structure of the imidazolium cation on enhancement of the performance of Au electrodes in CO_2 reduction, and highlighted the importance of coordination of the C_2-proton to adsorbed CO_2, facilitating the first electron transfer step. Our study also demonstrated that among cations studied, the 1,3-dimethyl imidazolium (MM) cation induces close to the best performance of Au electrodes.[10]

Several research groups have investigated the performance of electrodes other than Au under anhydrous conditions. For instance, Vera et al. achieved a high Faradaic efficiency (FE) of up to 90% of oxalic acid for a Pb electrode in various non-aqueous solvents.[11] Meanwhile, Sacci et al. used CuSn alloys in a mixture of acetonitrile (MeCN) and butyl-methyl imidazolium cations, and report a FE in CO formation below 40%, likely due to difficulties in controlling the water content of the solvent.[12] By in situ spectro-electrochemical studies, Koper et al. demonstrated CO formation on Cu electrodes in MeCN, but the concomitant reduction of water at various overpotentials may have affected the results, and makes it difficult to quantify the reaction efficiency.[4a]

To determine trends in performance of late transition metals in CO_2 reduction in non-aqueous media, we conducted electrochemical experiments in carefully prepared, dry acetonitrile

[a] S. Neyrizi, Prof. Dr. G. Mul
Photocatalytic Synthesis Group, Faculty of Science & Technology of the University of Twente, PO Box 217, Enschede, The Netherlands
E-mail: g.mul@utwente.nl

[b] S. Neyrizi, Dr. M. A. Hempenius
Sustainable Polymer Chemistry, Faculty of Science & Technology of the University of Twente, PO Box 217, Enschede, The Netherlands

Supporting information for this article is available on the WWW under https://doi.org/10.1002/celc.202300383

solutions containing 1,3-dimethyl imidazolium cations to enhance the performance of the electrodes. We demonstrate a volcano relationship between the CO_2 reduction rate, and the CO binding energy, and also elaborate on differences in CO_2 binding energy between Au, Zn and Cu, as determined by density functional theory (DFT) calculations. Finally, we compare the observed volcano trend in non-aqueous and aqueous conditions, and discuss (quantitative) differences on the basis of the role of the imidazolium cations in stimulating reduction of CO_2.

Results and Discussion

Figure 1 presents the results of CO_2 electrolysis for five, commercially available, polycrystalline metal electrodes. The chronopotentiometry curves were obtained using 0.5 mol% 1,3-dimethylimidazolium bis(trifluoromethylsulfonyl)imide (MM NTf_2) in acetonitrile (MeCN), with anhydrous conditions ensured via a rigorous protocol (see Experimental Section). All five metals (Ni, Cu, Au, Ag, and Zn) exhibit close to 100% Faradaic efficiency (FE) to CO. We also evaluated the performance of an Fe electrode (see Figure S6a). The Fe electrode was almost inactive for CO_2 reduction in the imidazolium-anhydrous MeCN electrolyte, likely due to CO poisoning of the surface. The current observed for Fe electrodes is likely caused by reduction of acetonitrile. A LSV in a similar potential range is shown for the Au electrode in Figure S6b. The figure clearly shows a considerable difference in the potential-current profiles under CO_2 and He purge, with a notably larger Faradaic current around −2.0 V (vs. Ag/Ag^+) under CO_2 atmosphere, exclusively assigned to production of CO.

The stability of the Ni electrode was visually assessed as shown in Figure S7. In both images, the Ni surface appears clean and the solution is clear. The stability of the Au electrode in CO production was examined at −10 mA/cm^2 and is shown in Figure S8. A sustained high FE towards CO was observed. Subsequent NMR analyses (see Figures S9–S14) of the electrolyte corroborates these findings, confirming that both MM NTf_2 and acetonitrile remain unchanged after electrolysis using Ni or Au electrodes.

Although many studies have reported high FEs for CO formation using Ag and Au electrodes, particularly in aqueous media, to the best of our knowledge, this is the first study to demonstrate close to 100% FE for CO formation with polycrystalline Ni, Zn, and Cu electrodes.[13] The study also uncovers an intriguing trend in the CO_2 reduction activity of the various transition metal catalysts under near-steady-state conditions for 5 hours. In particular, Au exhibits the highest activity, requiring the lowest potential to achieve the same current density, while Cu and Ag displayed nearly identical performance. Conversely, Zn and Ni demonstrate the lowest activity. This finding offers valuable insights into the efficacy of different metals as catalysts for CO_2 reduction in non-aqueous media. Jaramillo and co-workers performed a similar comparison of metal electrodes in aqueous media, reporting CO_2 reduction activity for several transition metal catalysts.[1] In their study, Au and Ag were the only catalysts showing a FE greater than 90 percent for CO_2 reduction. Zn and Cu showed, respectively, 80% and 68% FE for products of CO_2 reduction (the remaining FE was assigned to the formation of H_2), and Ni was reported to display a FE less than 5% for CO_2 reduction with most of the electrons utilized for H_2 evolution. These results highlight that an electrolyte composed of anhydrous MeCN and imidazolium cations provides favorable kinetics for the reduction of CO_2 to CO,

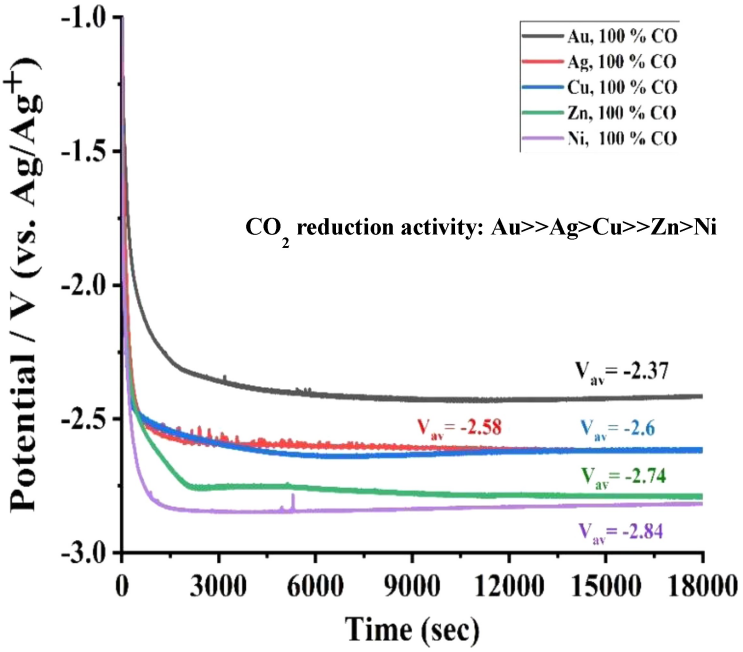

Figure 1. Electrolysis results for CO_2 reduction at −1 mA/cm^2 for 5 different transition metal catalysts in anhydrous acetonitrile, containing 0.5 mol% of MM NTf_2. Additional information regarding gas analysis and evaluation of Faradaic efficiencies can be found in Supporting Information Section III.

including metals such as Ni, typically producing H_2 in CO_2 containing aqueous electrolytes.

To support results from electrolysis experiments, Figure 2 (left) shows the LSV results for all five electrodes under CO_2 atmosphere. Cu shows the lowest overpotential, but shows a distinctively different, shallow i-V curve. To further support the i-V curve of the Cu electrode for CO_2 reduction, comparison of LSV results under a purge of He or CO_2 are also displayed (Figure 2, right). Although less evident, also for Ni the i-V curve is shallower in comparison to the other metals, with Au clearly showing the highest current densities at equivalent potentials. The shape of the LSV curves of Cu and Ni could suggest a possible difference in the CO_2 reduction mechanism for these two catalysts in comparison to the other metals investigated. The results obtained during He purge (Supporting Information Figure S15) demonstrate a remarkably similar activity for Au, Zn, and Ni electrodes, with onset potentials at approximately −2.4 V (vs. Ag/Ag^+). This observation indicates that the reduction of imidazolium is not influenced by the nature of the electrode, suggesting it is most likely a non-catalytic reductive process. This reinforces the notion that the variation in CO_2 reduction activity among different transition metals should be explained by variations in the interaction of the electrode with the CO_2 (reactant) or CO (product) molecules.

To further explore these differences, we employed DFT calculations to determine the binding energies of CO for a range of metals. We then compared these energies with CO_2 reduction activities obtained through experiments (as depicted in Figure 3a).

Upon analyzing the results presented in Figure 3a, a volcano relationship between the CO binding energy and the overall CO_2 reduction activities in anhydrous acetonitrile can be drawn. Specifically, we observe that Au is located at the apex of the volcano, exhibiting a favorable binding energy for CO resulting in the highest CO_2 reduction activity among the catalysts tested. To explain the difference in performance of Au and Zn, a metal with a low CO binding strength, we further explored the interaction of CO_2 with a negatively charged Au surface, as well as a negatively charged Zn surface. Figure 4 illustrates the interaction of CO_2 molecule with the metal surfaces, which are located at the same distance from the on-top metal atoms. The analysis shows that the transfer of the partially negative charge to CO_2 molecule is more prominent in the presence of the Au surface compared to the Zn surface. The charge transfer from the negatively charged Zn slab to the CO_2 molecule is found to be rather insignificant and even of opposite sign ($\delta(CO_2)$: +0.002) compared to that of Au ($\delta(CO_2)$: −0.241), which can explain the lower activity for CO_2 reduction on Zn. In addition, we performed DFTB calculations to investigate the intrinsic affinity of the two metal slabs with the CO_2 molecule in the absence of negative charge. The results reveal that CO_2 also has a stronger interaction with a neutral Au slab compared to a neutral Zn slab, resulting in a shorter equilibrium distance and a smaller OCO bond angle (as summarized at the top of Figure 4). These findings suggest that the affinity of Zn metal towards CO_2 is noticeably lower than that of Au, which can be attributed to differences in their electronic properties and surface energies.[14] The results presented in Figure 4 lend support to the hypothesis that the initial electron transfer to adsorbed CO_2 represents the rate-determining step for catalysts located on the left side of the volcano plot, associated with a relatively steep i-V slope, as depicted in Figure 3c.

Metals such as Cu and Ni, which exhibit stronger binding to CO than Au, also exhibit slow kinetics[15] To gain deeper insights into the interaction between CO and Au and CO and Cu (a catalyst located on the right side of Au in the volcano plot), we utilized DFT calculations to analyze the Mulliken population of CO on negatively charged Cu and Au slabs (Figure 5). A larger (partial) negative charge on the CO molecule can be calculated for the Cu slab than for the Au slab ((δ(CO): −0.105 for Cu versus (δ(CO): −0.072 for Au). A high negative value agrees with a strong interaction of CO with metal atoms, and thus agrees with a relatively high energy required for CO desorption. Electronic models, such as the d-band model, which leverage the electronic properties of the metal, particularly the d-band center (ε_d), have previously been successfully utilized to predict

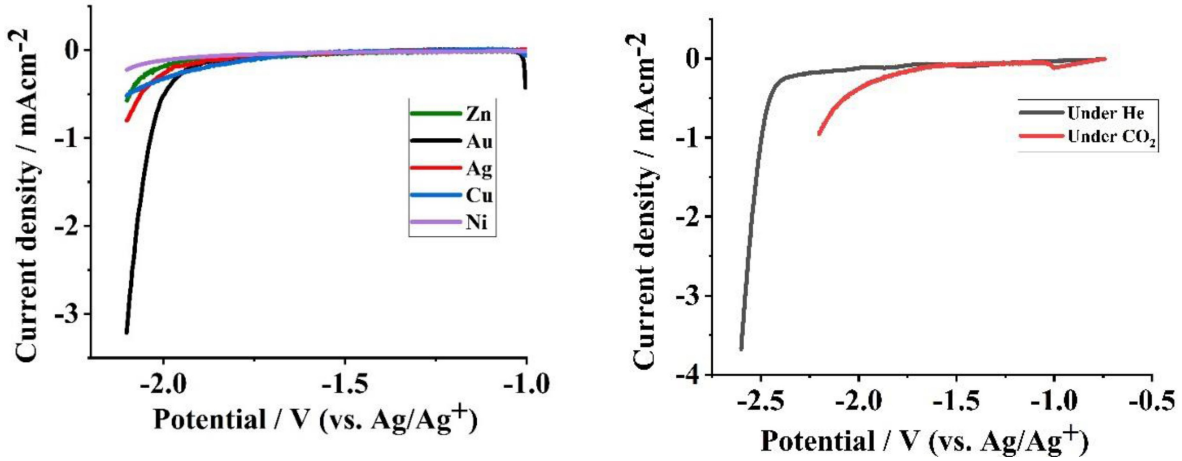

Figure 2. Left: LSV results for CO_2 reduction for 5 different transition metal catalysts in anhydrous acetonitrile. 0.5 mol% of MM NTf_2 was used as both electrolyte and co-catalyst. Right: comparison of LSV results for Cu electrode under He and CO_2 purging.

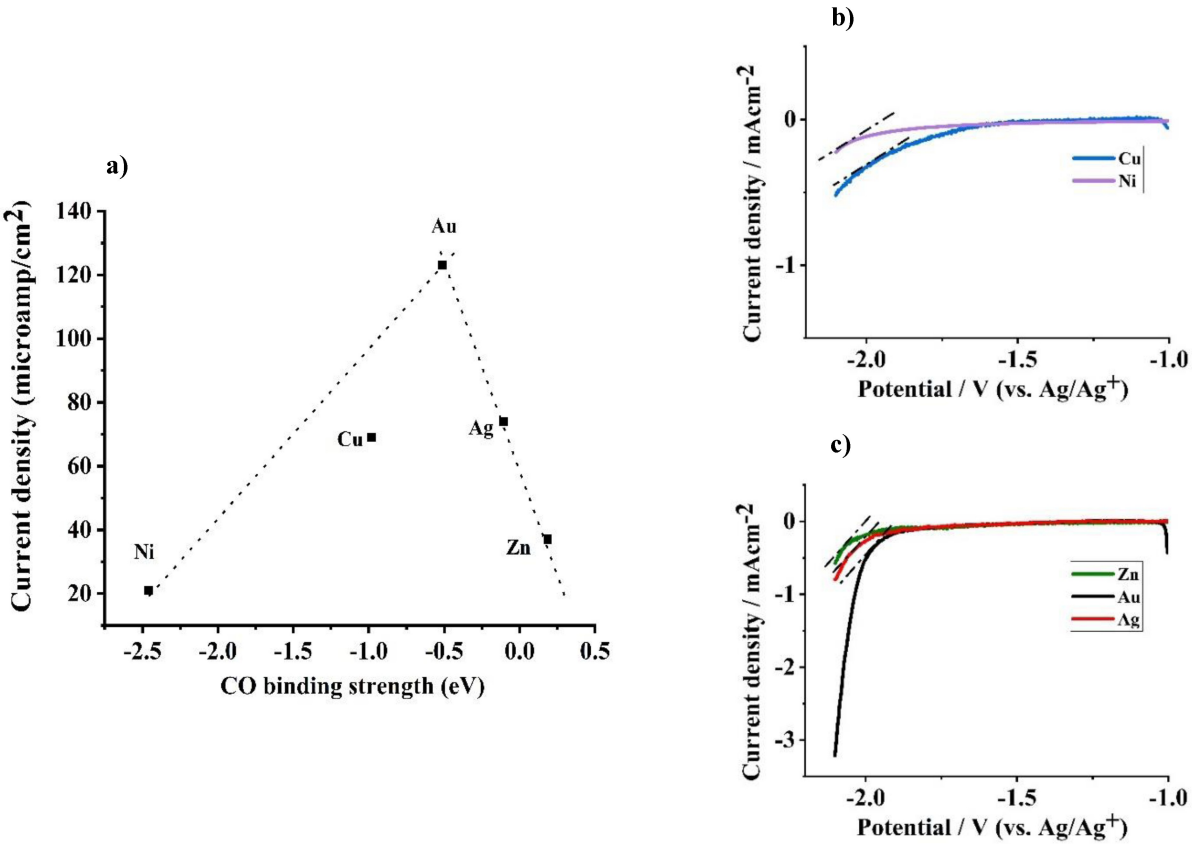

Figure 3. (a) Volcano plot illustrating current density obtained from chronopotentiometry data under stirring conditions for CO_2 reduction at −2 V versus CO binding strength. Results are normalized against geometric surface area, (b) LSVs for Ni and Cu electrodes; and (c) LSVs for Zn, Au, and Ag electrodes for CO_2 reduction in anhydrous acetonitrile in quiescent solutions with a CO_2 flow rate of 5 ml/min. In all experiments 0.5 mol% of MM NTf_2 was used as both electrolyte and catalyst. Please note that the steady state current densities used for Figure 3a are lower than observed in the respective LSVs, likely due to build-up of adsorbed species on the electrode surface and an associated charge transfer resistance.

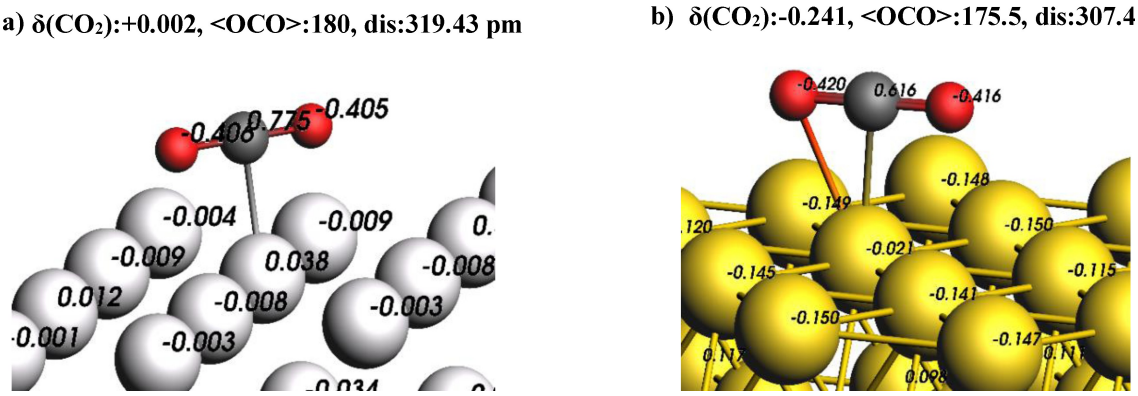

Figure 4. Mulliken population analysis for CO_2 interacting with negatively charged metal slabs, calculated using single-point BAND calculations. Subfigures (a) and (b) illustrate the results for CO_2 interacting with Zn and Au slabs, respectively. The figure highlights the charge differences between the top metal atom and its surroundings, as well as the negative charges found on oxygen atoms and positive charges found on carbon atoms. The figure highlights the results for charge transfer ($\delta(CO_2)$) from BAND calculations, along with the CO_2 bond angle (OCO) and the equilibrium distance from the surface (dis: in picometer) from DFTB calculations, which are summarized at the top.

CO binding energies with transition metals.[16] Our conclusion is in agreement with previous studies, which also demonstrate that Cu, Ni, Pt, and Fe catalysts have stronger interactions with CO than Au.[16] The Volcano plot presented in this study serves as a useful tool for predicting the reactivity of transition metal catalysts in non-aqueous CO_2 reduction based on their CO adsorption.

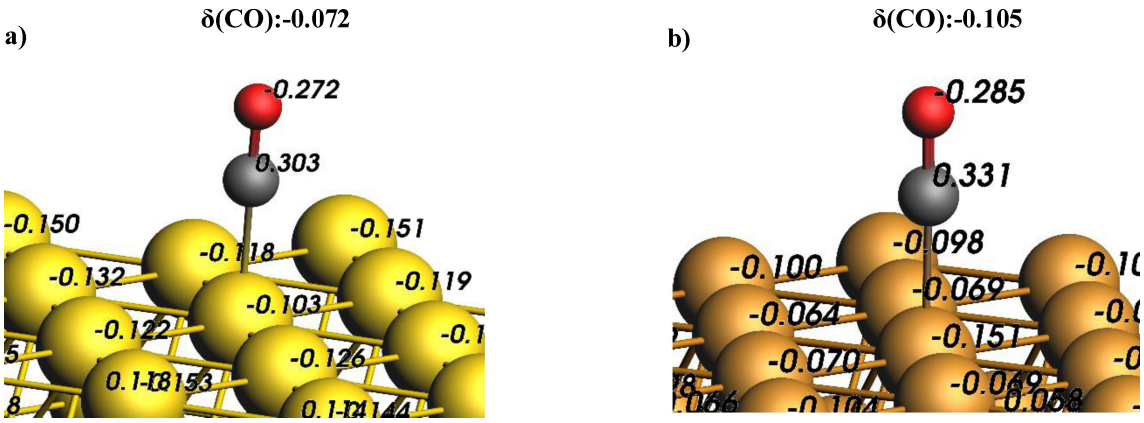

Figure 5. Mulliken population analysis for CO interacting with negatively charged metal slabs, calculated using single-point BAND calculations. Subfigures (a) and (b) illustrate the results for CO interacting with Au and Cu slabs, respectively. The figure highlights the charge differences between the top metal atom and its surroundings, as well as the negative charges found on oxygen atoms and positive charges found on carbon atoms. Details of charge transfer results are also summarized at the top.

Comparing Dry Acetonitrile to Aqueous Conditions

A similar volcano plot shown in Figure 3 for dry acetonitrile (containing imidazolium salt), has previously been reported for aqueous conditions by Jaramillo and colleagues.[1] The two volcano plots are compared in Figure 6. In aqueous conditions, Jaramillo and coworkers observed orders of magnitude differences (see the logarithmic scale) in activity when comparing Au to other metals, such as Ag, Cu, and Ni, much more significantly than in our non-aqueous conditions. For example, Jaramillo and colleagues find performance ratios of Au/Ag ~10 and Au/Zn ~100 for the current density associated with CO_2 reduction at equivalent potential (Figure 6, right). However, in MeCN-imidazolium-assisted CO_2 reduction, the difference between the activities of different electrodes is much smaller (Figure 6, left). For example, the Au/Ag ratio for the activity (the performance factor) reported in our work is only ~1.6, and the Au/Zn performance factor ~3.6. Besides the significantly suppressed evolution of H_2 for Ni and Zn catalysts, we propose that the smaller factor is associated with mediation by imidazolium cations. In previous work, we conducted a comprehensive investigation using inverse kinetic isotope effect analysis, Tafel plot measurements, and (DFT) calculations to examine the impact of the imidazolium cation on the pathway of CO_2 electrochemical reduction over Au electrodes in anhydrous acetonitrile. Our findings revealed a notable influence of the

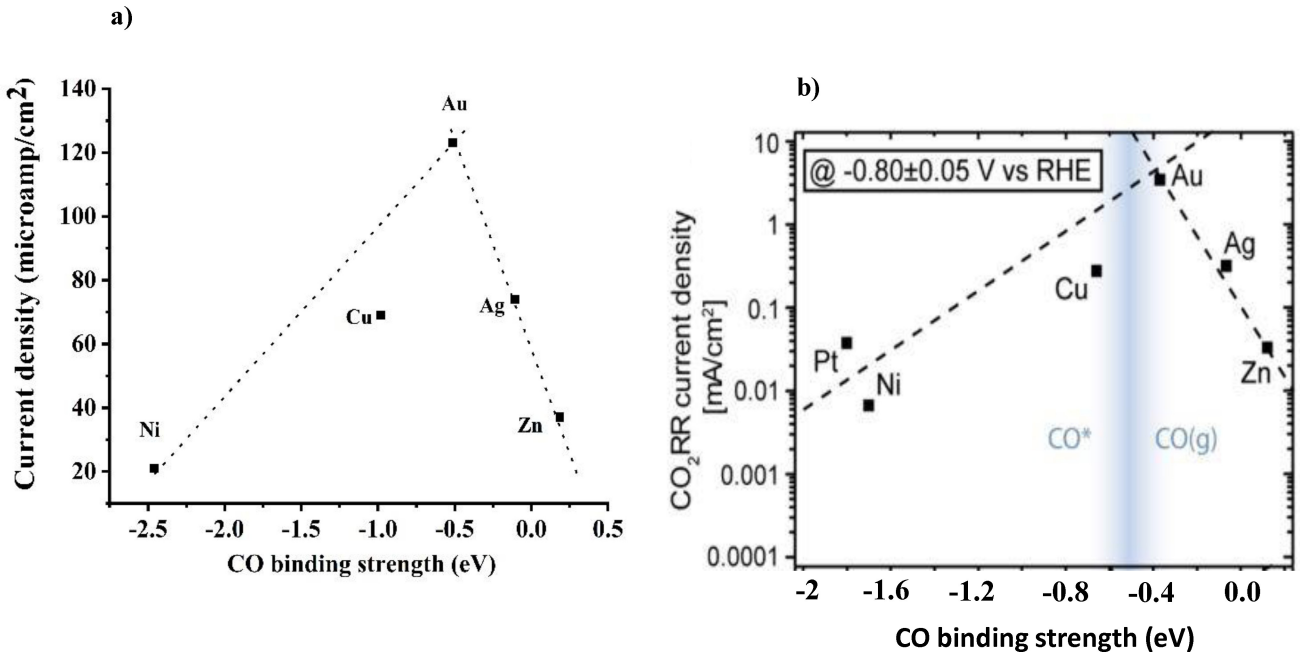

Figure 6. Volcano plot of CO_2 reduction activity for transition metal catalysts. (a) obtained in this work for anhydrous MeCN and 0.5 % mol MM NTf_2 as promotor, see caption for Figure 3a. (b) obtained for aqueous media from the work of Jaramillo et al.[1]

imidazolium cation on the electron density of the negatively charged adsorbed CO_2 species. Specifically, our results demonstrate that the presence of imidazolium cations leads to a lower energy barrier for the formation of highly polarized adsorbed $*CO_2^-$ species, achieved through the interaction with the C2-proton of the cation.[10] Thus, the primary cause of the differences in activity between various transition metal catalysts examined in this study, especially those with high energy barriers for CO_2 adsorption (such as the Zn, Au, and Ag electrodes), is expected to be the mediation of the first electron transfer step by H-bond formation with the imidazolium cation.

We like to mention, however, that the impact of the imidazolium cation on the CO desorption energies of various metals, should also be taken into consideration. Yet, a simplified microkinetic model presented in the Supporting Information demonstrates that chemical adsorption of CO_2 plays the dominant role in determination of the overall reaction rate, even for catalysts where CO desorption is inhibiting.

An intriguing aspect of utilizing the imidazolium-acetonitrile electrolyte for CO_2 reduction is gaining a comprehensive understanding of the overall electrochemical process, including the anodic reaction. Since we have used very dry conditions, we propose the cathodic reaction involves 2 CO_2 molecules, one which is the oxygen donor, and the other the oxygen acceptor, as discussed by Hu and coworkers, citing earlier work of Savéant [Reaction (1)].[17]

$$2e + 2\ CO_2 \rightarrow CO + CO_3^{2-} \quad (1)$$

Notably, we did not detect bulk formation of carbonate species in our small-scale reactor, and NMR analysis conducted after electrolysis showed no evidence of water formation (refer to Supporting Information Figures S9–S14). These findings suggest that CO_3^{2-} is anodically converted by Reaction (2) over graphite electrodes:

$$CO_3^{2-} \rightarrow CO + O_2 + 2e \quad (2)$$

Anodic oxidation of carbonate has recently been proposed to play a major role in the anodic production of H_2O_2 and formation of O_2 by oxidation of carbonate has also been observed in aqueous conditions.[18] However, a thorough and dedicated analysis is required to examine anodic reactions, which is recommended for future research.

Conclusions

In summary, our investigation demonstrates the high potential of imidazolium co-catalyzed CO_2 reduction in dry acetonitrile using late-transition metal catalysts. Our findings highlight the high Faradaic efficiency towards CO of non-expensive metals such as Zn, Cu, and Ni in anhydrous acetonitrile, which in combination with the CO_2 absorption capacity of acetonitrile could lead to efficient CO_2 reduction systems. Additionally, our observation of a volcano relationship among late-transition metals, with Au showing the highest activity, provides valuable design principles for optimizing CO_2 reduction efficiency in non-aqueous solvents.

Experimental Section

Gold (Au) electrodes (3.0 mm diameter, 99.95%) were purchased from Prosense. Gold wire (0.25 mm diameter, 99.99%), Zn wire (1.0 mm diameter, 99.99%), Ni wire (0.5 mm diameter, 99.99%), Fe wire (1.0 mm diameter, 99.99%), Ag wire (0.25 mm diameter, 99.99%), and Cu foil (thickness 0.25 mm, 99.98%) were supplied by Sigma Aldrich. Anhydrous acetonitrile (99.8%), acetonitrile (ReagentPlus, 99%), silver trifluoromethanesulfonate (≥99%), acetonitrile-d3 (≥99.8 atom% D) were obtained from Sigma-Aldrich. Acetonitrile-d3 (99.8 atom % D) for electrolysis experiments was obtained from Acros Organics. 1,3-Dimethylimidazolium bis(trifluoromethylsulfonyl)imide (99%) was purchased from Iolitec Ionic Liquids Technologies GmbH. All chemicals were transferred to the glove box and were used without further treatment.

For each electrolysis measurement, the electrodes underwent an initial polishing process using sandpaper until a smooth and shiny surface was achieved. In the case of voltammetry electrodes, a polishing pad (Prosense, QVMF 1040) was moistened with ethanol and the electrode was gently polished for a duration of 4 minutes (no alumina was utilized on the polishing pad). Subsequently, the electrodes were thoroughly rinsed with Milli-Q water (Milli-Q® Reference, 18.2 MΩ, 5 ppb TCO, Merc) and subjected to 10-minute sonication in 0.5 molar HNO_3. Following this step, another round of sonication in ethanol was performed, concluding with a 10-minute sonication in HPLC grade acetonitrile (99.9%, Sigma Aldrich) to ensure reproducibility of the pristine electrode surface. It is important to note that the electrodes were always rinsed with Milli-Q water between each sonication step. Figure S16 displays the results of SEM and EDX analysis from Ni and Au electrodes after the above-mentioned cleaning procedure.

The glass reactor, reference compartment, graphite rod, gas inlet, and gas outlet tubes underwent a thorough rinsing process using Milli-Q water, ethanol, and HPLC grade acetonitrile. Subsequently, the working electrode and all other reactor components were assembled, and the entire setup was sonicated for 2 sets of 5 minutes using HPLC grade acetonitrile. Following this step, the reactor was subjected to a continuous purge of super dry helium (Helium A/Zero Grade N4.6, Linde) for a duration of 30 minutes prior to the introduction of the electrolyte. In experiments involving CO_2, a dryer (Z Pure DS H_2O, ChromRes) was employed to ensure the complete removal of moisture from the CO_2 inlet (Carbon Dioxide Food Grade, Linde) before it entered the reactor. This additional step ensured that the CO_2 supplied to the reactor was free from any residual moisture.

For all measurements, a Ag wire was used as the pseudo-reference electrode. A 1 mol% Ag OTf in 0.1 mL anhydrous acetonitrile was always used as the reference solution and was separated from the working solution with an ASTM ultrafine frit. Working solutions always contained 0.5 mol% of the electrolyte and were all prepared inside the glove box. NTf_2 was used as the common electrolyte anion and anhydrous acetonitrile was the common solvent for all measurements. A graphite rod (99.99% Sigma Aldrich) was used as the counter electrode. Gas chromatography (Compact GC 4.0, Inter science) was used to analyze the gas products from the reactor. He was used as the carrier gas and the GC was calibrated for 1 to 100,000 ppm CO (Carbon Monoxide CP Grade N3.0, Linde). All electrochemical measurements were performed with a Biologic SP-300 potentiostat in a three-electrode configuration. For all measurements, the flow of the gas inlet was 5 mL/min and LSVs were

recorded in quiescent solution to keep the hydrodynamic conditions the same. Before any electrochemical measurement, we made sure that a stable open-circuit voltage was established.

Supporting Information

The authors have cited additional references within the Supporting Information.[19]

Acknowledgements

This work is part of the Advanced Research Center for Chemical Building Blocks, ARC CBBC, which is co-founded and co-financed by the Dutch Research Council (NWO) and the Netherlands Ministry of Economic Affairs and Climate Policy. We thank Shell Global Solutions International B.V. for financial and technical support. Karl-Fischer titrations and some GC analyses were performed in collaboration with Shell Global Solutions International B.V.

Conflict of Interests

The authors declare no conflict of interest.

Data Availability Statement

Electrochemical data, detailed information about DFT calculations, gas and liquid analysis data are provided in the Supporting Information.

Keywords: carbon dioxide · électrodes · imidazolium · acetonitrile · carbon monoxide

[1] K. P. Kuhl, T. Hatsukade, E. R. Cave, D. N. Abram, J. Kibsgaard, T. F. Jaramillo, *J. Am. Chem. Soc.* **2014**, *136*, 14107–14113.
[2] a) K. Liu, W. A. Smith, T. Burdyny, *ACS Energy Lett.* **2019**, *4*, 639–643; b) M. Ma, E. L. Clark, K. T. Therkildsen, S. Dalsgaard, I. Chorkendorff, B. Seger, *Energy Environ. Sci.* **2020**, *13*, 977–985; c) D. Higgins, C. Hahn, C. Xiang, T. F. Jaramillo, A. Z. Weber, *ACS Energy Lett.* **2019**, *4*, 317–324; d) M. Akira, H. Yoshio, *Bull. Chem. Soc. Jpn.* **1991**, *64*, 123–127; e) M. R. Singh, Y. Kwon, Y. Lum, J. W. Ager, A. T. Bell, *J. Am. Chem. Soc.* **2016**, *138*, 13006–13012; f) J. Resasco, L. D. Chen, E. Clark, C. Tsai, C. Hahn, T. F. Jaramillo, K. Chan, A. T. Bell, *J. Am. Chem. Soc.* **2017**, *139*, 11277–11287.
[3] a) Y. Y. Birdja, E. Pérez-Gallent, M. C. Figueiredo, A. J. Göttle, F. Calle-Vallejo, M. T. M. Koper, *Nat. Energy* **2019**, *4*, 732–745; b) Z. Sun, T. Ma, H. Tao, Q. Fan, B. Han, *Chem* **2017**, *3*, 560–587.
[4] a) M. C. Figueiredo, I. Ledezma-Yanez, M. T. M. Koper, *ACS Catal.* **2016**, *6*, 2382–2392; b) J. W. Blake, J. T. Padding, J. W. Haverkort, *Electrochim. Acta* **2021**, *393*, 138987; c) Y. Matsubara, *ACS Energy Lett.* **2017**, *2*, 1886–1891.
[5] a) D. Wakerley, S. Lamaison, J. Wicks, A. Clemens, J. Feaster, D. Corral, S. A. Jaffer, A. Sarkar, M. Fontecave, E. B. Duoss, S. Baker, E. H. Sargent, T. F. Jaramillo, C. Hahn, *Nat. Energy* **2022**, *7*, 130–143; b) A. Wuttig, Y. Yoon, J. Ryu, Y. Surendranath, *J. Am. Chem. Soc.* **2017**, *139*, 17109–17113; c) S. Zhu, B. Jiang, W.-B. Cai, M. Shao, *J. Am. Chem. Soc.* **2017**, *139*, 15664–15667.
[6] a) A. Goyal, G. Marcandalli, V. A. Mints, M. T. M. Koper, *J. Am. Chem. Soc.* **2020**, *142*, 4154–4161; b) H. Ooka, M. C. Figueiredo, M. T. M. Koper, *Langmuir* **2017**, *33*, 9307–9313; c) C. W. Li, M. W. Kanan, *J. Am. Chem. Soc.* **2012**, *134*, 7231–7234; d) D. Ren, N. T. Wong, A. D. Handoko, Y. Huang, B. S. Yeo, *J. Phys. Chem. Lett.* **2016**, *7*, 20–24.
[7] C. Amatore, J. M. Saveant, *J. Am. Chem. Soc.* **1981**, *103*, 5021–5023.
[8] Y. Tomita, S. Teruya, O. Koga, Y. Hori, *J. Electrochem. Soc.* **2000**, *147*, 4164.
[9] a) G. P. S. Lau, M. Schreier, D. Vasilyev, R. Scopelliti, M. Grätzel, P. J. Dyson, *J. Am. Chem. Soc.* **2016**, *138*, 7820–7823; b) A. Kemna, N. García Rey, B. Braunschweig, *ACS Catal.* **2019**, *9*, 6284–6292; c) B. A. Rosen, J. L. Haan, P. Mukherjee, B. Braunschweig, W. Zhu, A. Salehi-Khojin, D. D. Dlott, R. I. Masel, *J. Phys. Chem. C* **2012**, *116*, 15307–15312; d) Sun, G. K. Ramesha, P. V. Kamat, J. F. Brennecke, *Langmuir* **2014**, *30*, 6302–6308; e) B. A. Rosen, A. Salehi-Khojin, M. R. Thorson, W. Zhu, D. T. Whipple, P. J. A. Kenis, R. I. Masel, *Science* **2011**, *334*, 643–644.
[10] S. Neyrizi, J. Kiewiet, M. A. Hempenius, G. Mul, *ACS Energy Lett.* **2022**, *7*, 3439–3446.
[11] V. Boor, J. E. B. M. Frijns, E. Perez-Gallent, E. Giling, A. T. Laitinen, E. L. V. Goetheer, L. J. P. van den Broeke, R. Kortlever, W. de Jong, O. A. Moultos, T. J. H. Vlugt, M. Ramdin, *Ind. Eng. Chem. Res.* **2022**, *61*, 14837–14846.
[12] R. L. Sacci, S. Velardo, L. Xiong, D. A. Lutterman, J. Rosenthal, *Energies* **2019**, *12*, 3132.
[13] a) Y. Hori, H. Wakebe, T. Tsukamoto, O. Koga, *Electrochim. Acta* **1994**, *39*, 1833–1839; b) D. Gao, Y. Zhang, Z. Zhou, F. Cai, X. Zhao, W. Huang, Y. Li, J. Zhu, P. Liu, F. Yang, G. Wang, X. Bao, *J. Am. Chem. Soc.* **2017**, *139*, 5652–5655; c) Y. Hori, in *Modern Aspects of Electrochemistry* (Eds.: C. G. Vayenas, R. E. White, M. E. Gamboa-Aldeco), Springer New York, New York, NY, **2008**, pp. 89–189.
[14] B. Hammer, J. K. Nørskov, in *Advances in Catalysis, Vol. 45*, Academic Press, **2000**, pp. 71–129.
[15] a) H. Yoshio, K. Osamu, A. Akiko, E. Michio, *Bull. Chem. Soc. Jpn.* **1992**, *65*, 3008–3010; b) O. Koga, T. Matsuo, H. Yamazaki, Y. Hori, *Bull. Chem. Soc. Jpn.* **1998**, *71*, 315–320; c) S. A. Akhade, W. Luo, X. Nie, N. J. Bernstein, A. Asthagiri, M. J. Janik, *Phys. Chem. Chem. Phys.* **2014**, *16*, 20429–20435.
[16] a) J. K. Nørskov, F. Abild-Pedersen, F. Studt, T. Bligaard, *Proc. Natl. Acad. Sci. USA* **2011**, *108*, 937–943; b) B. Hammer, Y. Morikawa, J. K. Nørskov, *Phys. Rev. Lett.* **1996**, *76*, 2141–2144.
[17] Y. Oh, H. Vrubel, S. Guidoux, X. Hu, *Chem. Commun.* **2014**, *50*, 3878–3881.
[18] J. Zhang, C. W. Oloman, *J. Appl. Electrochem.* **2005**, *35*, 945–953.
[19] a) S. Grimme, C. Bannwarth, P. Shushkov, *J. Chem. Theory Comput.* **2017**, *13*, 1989–2009; b) M. Franchini, P. H. T. Philipsen, E. van Lenthe, L. Visscher, *J. Chem. Theory Comput.* **2014**, *10*, 1994–2004; c) G. Wiesenekker, G. t. Velde, E. J. Baerends, *J. Phys. C* **1988**, *21*, 4263; d) E. Van Lenthe, E. J. Baerends, *J. Comput. Chem.* **2003**, *24*, 1142–1156.

Manuscript received: August 2, 2023
Revised manuscript received: October 16, 2023
Version of record online: April 15, 2024